Miniaturized Detection System for Fluorescence and Absorbance Measurements in Chromatographic Applications

Sara Van Overmeire, Heidi Ottevaere, Gert Desmet, and Hugo Thienpont, *Associate Member, IEEE*

***Abstract*—We present a microoptical detection unit for both laser-induced fluorescence and absorbance analysis on fused silica capillaries, which can be used for chromatographic applications. The detection system is designed by means of nonsequential ray tracing simulations and prototyped by means of deep proton writing. In a proof-of-concept demonstration, the microoptical unit is used for the detection of various concentrations of coumarin dyes. The detection limit (SNR = 3.3) achieved measures 0.6 nM for fluorescence analysis and 12 μM for absorbance measurements in capillaries with an inner diameter of 150 μm.**

***Index Terms*—Absorbance, chromatography, fluorescence, optics, plastics, rapid prototyping.**

I. Introduction

CHROMATOGRAPHY—a collection of laboratory techniques for the separation of mixtures of fluids or gases—is ubiquitous in today's scientific world. Ideally the results of a sample analysis should be available instantly and in the field (e.g., a toxicologist at the riverside, a physician visiting a patient). Yet, this is not possible with the present expensive and bulky commercial chromatographic systems. Therefore, scientists shift to microchromatographic systems: very small analysis systems that can provide results very fast and with a reasonable resolution.

Over the last few decades, various micro total analysis systems (μTAS)—also called lab-on-a-chip, miniaturized, or microfluidic analysis systems—have been developed, which integrate different chemical processes (sample pretreatment, mixing, chromatographic, or electrophoresis separation) on a single chip [1], [2]. Miniaturization of these analytical process steps improves the system's performance and speed drastically. Additionally, miniaturization enables a size reduction of the chemical system and a significant decrease of reagent and sample consumption, which makes them suitable for use in the field. Finally, several systems can be combined on one substrate to enable parallel investigation. However, up to now, conventional, bulky, and expensive detection systems have to be employed to detect the minute amounts of molecules in the microchannels on these chips. There exists a strong need for miniaturized and integrated on-chip detection units, which are lightweight, low cost, reliable, robust, and simple to operate, and which have a high processing speed. These systems will enable the development of portable, robust, and, ultimately, disposable μTAS systems that can be used in the field and for point-of-care applications.

Due to its selectivity and high sensitivity, laser-induced fluorescence (LIF) is one of the preferred detection techniques on microchemical chips. The macroscopic confocal LIF configuration enables highly sensitive detection on microchips: detection limits of the order of a few picomolar (pM) down to 300 femtomolar (fM) have been realized [3], [4]. However, by using a nonconfocal setup with macroscopic optical components, pM detection limits can also be obtained [5]. Several (partly) miniaturized and integrated systems for nonconfocal LIF detection have already been developed and employed in microfluidic analysis systems [6]–[12]. The reported detection limits in these miniaturized and integrated systems are usually in the nanomolar range, i.e., three orders of magnitude higher than those obtained in the macroscopic LIF systems. Therefore, we can conclude that the nonconfocal architectures are promising, but further optimization of the miniaturization and integration of the optical components is needed to be able to offer a valuable miniaturized alternative to the classical confocal macroscopic setup. We should remark that not all reported detection limits were defined in a similar way. As further discussed in Section IV, the detection limit is defined as the smallest concentration of molecules that can be detected with a signal-to-noise ratio (SNR) of at least 3.3. Some authors, however, use an SNR of 2 to calculate the detection limit of their system. In addition, flow rate of the sample in the channel under test, the detection volume, which is analyzed by the system, the chosen fluorescent dye, the quantum efficiency of the dye at the chosen excitation wavelength, and the length or the volume of the plugs of molecules that need to be analyzed, will all influence the performance of the system. Consequently, a detailed comparison of different systems is not straightforward and should be carried out carefully.

One of the disadvantages of LIF is the need for chemical derivation of the molecules under test, which are usually not

Manuscript received October 7, 2007; revised October 22, 2007. This work was supported in part by the DWTC-IAP, in part by the FWO, in part by the GOA, in part by the 6th FP European Network of Excellence on Micro-Optics (NEMO), and in part by the OZR of the Vrije Universiteit Brussel. The work of S. Van Overmeire and H. Ottevaere was supported by the Flemish Fund for Scientific Research (FWO) which provided them respectively an "Aspirant" fellowship and a "Postdoctoraal Onderzoeker" fellowship.

S. Van Overmeire, H. Ottevaere, and H. Thienpont are with the Department of Applied Physics and Photonics (FirW-TONA), Vrije Universiteit Brussel, B-1050 Brussels, Belgium (e-mail: svoverme@vub.ac.be; hottevaere@vub.ac.be; hthienpo@vub.ac.be).

G. Desmet is with the Department of Chemical Engineering (FirW-CHIS), Vrije Universiteit Brussel, B-1050 Brussels, Belgium (e-mail: gedesmet@vub.ac.be).

Color versions of one or more of the figures in this paper are available online at http://ieeexplore.ieee.org.

Digital Object Identifier 10.1109/JSTQE.2007.912753

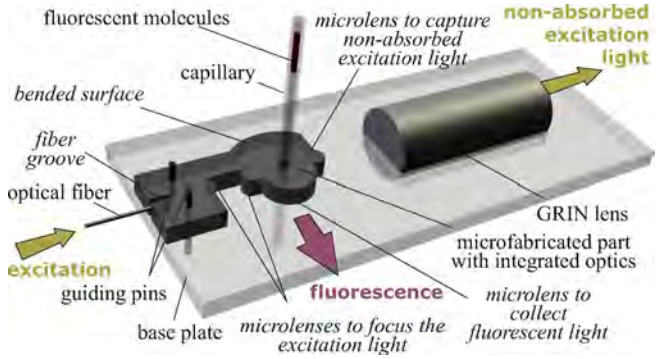

Fig. 1. Schematic representation of the complete detection unit.

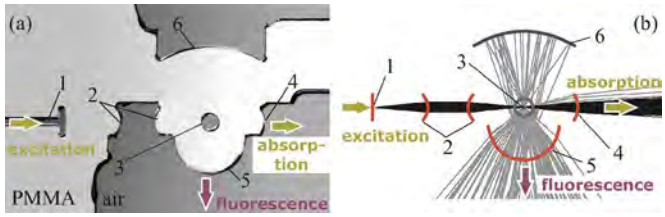

Fig. 2. (a) Image of the optical system and (b) schematic representation with ray tracing. (1 = fiber groove/fiber source, 2 = microlenses to focus the excitation light, 3 = hole to insert the capillary, 4 = microlens to capture nonabsorbed excitation light, 5 = microlens to collect fluorescence, and 6 = extra-bended reflective surface).

autofluorescent. UV-visible absorbance detection, on the other hand, does not need these chemical pretreatment steps and has a wider applicability. However, it suffers from high detection limits due to the short optical path length available in commonly used microchannels, and so, up to now, LIF detection has been the principal detection method employed. Yet, some attempts have been made to perform absorbance measurements in capillaries or on-chip microchannels [13]–[16]. Often, complex capillary geometries like, e.g., Z-cells, bubble cells, U-cells, or multireflection cells are implemented to increase the optical path length at the detection point [10], [17]–[22]. The reported detection limits in these miniaturized absorbance detection systems are usually in the micromolar range.

In this paper, we present a detection system with integrated optics for both fluorescence and absorbance measurements in capillaries for analytical chromatography. In one system, we combine highly sensitive fluorescence measurements of small concentrations of labeled molecules, with absorbance measurements of samples with higher concentrations but without the need for labeling. The goal is to focus on the advantage of using a microfabrication technology to directly integrate and align both the fluorescence and the absorbance detection system onto the microfluidic channel. The complete detection unit, as shown in Fig. 1 consists of a microfabricated part with integrated optics and a partly microfabricated and partly milled base plate for the alignment of the former microsystem with additional optics. The microfabricated part contains a groove to insert a fiber delivering the excitation light to the detection unit, integrated lenses, and a hole to insert a capillary, which will deliver the chemical sample. By integration, a perfect alignment of the microoptics and the excitation source with the microfluidic channel is assured. The microfabricated part also contains holes for guiding pins. Similar holes on corresponding positions will be provided in the base plate to align both systems with respect to each other. The base plate also contains a hole for the capillary and milled grooves to position additional lenses for which the alignment is not that critical, e.g., an extra GRIN lens for the absorption measurement.

Capillaries with different inner diameters can be inserted to study different optical path lengths. As the outer diameter of all capillaries is 360 μm, the design of the system remains the same and the same detection unit can be used. The capillaries themselves can contain the stationary phase needed for chromatographic separation, and thus, also serve as the chromatographic column. Alternatively, they can provide a coupling between a separate chromatographic system and the detector. In this paper, we present the proof-of-concept of the proposed detection configuration by using capillaries that can be easily replaced, but ultimately, the goal will be to adapt this detection approach for the detection of fluorescence and/or absorbance in microchannels with inner diameters ranging from a few micrometers up to 100 μm and special geometries like *Z*-cells to increase the optical path length at the detection point. Chromatographic separation will then be carried out on the same microfluidic chip, by which a true μTAS system can be created.

In Section II, we will discuss the design of the detection system by means of nonsequential ray tracing simulations. In Section III, the microfabrication technology deep proton writing (DPW) used to prototype our detection system will be introduced, and in Section IV, we discuss the use of the microoptical unit in a proof-of-concept demonstration setup for the detection of various concentrations of coumarin dyes. Finally, in Section V, we draw conclusions and formulate some approaches to increase the performance of our system in the future.

II. Design

The studied optical system (Fig. 2) has three functions: focusing of the incoming excitation laser beam onto the channel, detection of nonabsorbed excitation light, and collection of fluorescent light. For every function, we will describe the simulation strategy and the results obtained with ASAP, a commercial nonsequential optical ray-tracing program [23]. Nonsequential ray tracing was needed to take into account Fresnel reflections in the detection unit.

A. Excitation

The goal is to focus the excitation light by means of two cylindrical microlenses onto a small vertical line in the center of the capillary (Fig. 3). The excitation light with a wavelength of 409 nm is brought to the microoptical detection system by means of a single-mode optical fiber, which is placed as close as possible to the detection unit [poly-(methylmethacrylate) (PMMA)–air interface]. The light coming from the entrance fiber is propagated through the system and collected on a detector of

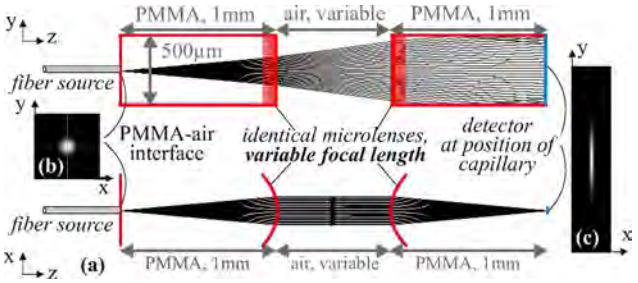

Fig. 3. (a) Schematic representation of the simulated setup and the obtained energy distribution of (b) the source (measurement area of 25 μm $\times$ 25 μm) and (c) at the position of the center of capillary (measurement area of 150 μm $\times$ 500 μm) (white = highest energy and black = lowest energy values).

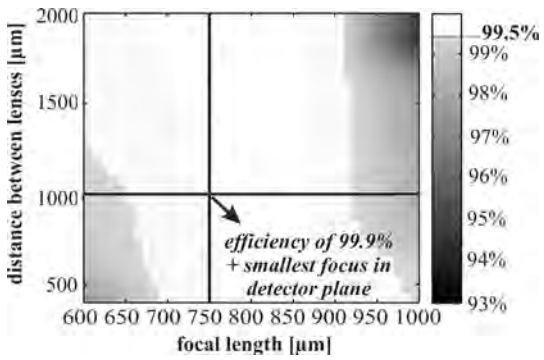

Fig. 4. Efficiency of the excitation as a function of the focal length of the microlenses and the distance between them.

150 μm (inner diameter of the capillary) $\times$500 μm at the position of the center of the capillary to investigate there the energy distribution of the light. PMMA was chosen for the microlenses, as this is the material for which the fabrication technology DPW is optimized (see Section III). The thickness of the system in the *y*-direction measures 500 μm, which is also determined by the DPW technology. The dimensions of the system in the *xz*-plane are summarized in Fig. 3. The system should be large enough to provide mechanical stability, but, on the other hand, the divergence of the light coming from the fiber tip in the *y*-direction should be limited. There are two variables in the system, the focal length of the microlenses and the distance between them, and in Fig. 4, we summarize their influence on the efficiency of the excitation, which is defined as the integrated energy distribution on the detector [Fig. 3(c)] divided by the integrated energy distribution of the source [Fig. 3(b)]. We can conclude that the system with two microlenses is a tolerant system, as there is a large region where the efficiency exceeds 99.5%. In this set of solutions, we select only those where the distance between the lenses measures 1 mm and we investigate the width of the energy distribution in cross sections along the *x*-direction in the center of the detector plane for various focal lengths (Fig. 5). The smallest focus is achieved with microlenses with a focal length of 750 μm and the resulting efficiency amounts to 99.9%. All previous simulations were done with ideal transmitting lens surfaces. In practice, no antireflection coating will be applied in a first step and Fresnel reflections will occur. By implementing these reflections in ASAP, the efficiency was lowered to 88.9%.

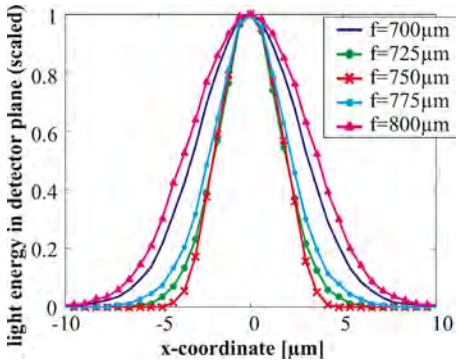

Fig. 5. Cross sections in *x*-direction of the energy distribution in the center of the detector plane for different focal lengths of the microlenses (the distance between the lenses measures 1 mm).

B. Absorbance

To measure absorption of molecules, the nonabsorbed excitation light that propagates through the capillary toward a detector should be quantified. In our system, we couple the nonabsorbed excitation light first into a multimode optical fiber (MMF), which guides the light then to the detector. An MMF was chosen, as it has a larger numerical aperture than a single-mode fiber (SMF). To focus the nonabsorbed excitation light onto the MMF, cylindrical microlenses with their curvature in the same plane (*xz*-plane in Fig. 3) like we used for the excitation, will not be sufficient. Indeed, in the plane perpendicular to the plane of curvature (*yz*-plane), diffraction will spread the light coming from the fiber source. Therefore, we need to provide in both planes one or more curved lens surface to focus the light onto the MMF, with different focusing properties in the two planes. We would not need such accurate microoptics to focus the light on a macrodetector in close proximity to the capillary without the optical fiber between them, but this detector would also collect a large amount of fluorescent light, which would increase the noise level for the absorbance measurement.

To enable focusing in both the *xz*- and the *yz*-plane, we opt for the combination of one refractive cylindrical and one spherical GRIN lens, instead of two cylindrical microlenses with each a different curvature and with their curvatures placed perpendicular to each other. By this, the smaller focal length in the *xz*-plane is implemented by means of a combination of two lenses, and thus, the system will be more tolerant for errors on their parameters. The advantage of a GRIN lens compared to a refractive spherical lens is its easy mounting and adjustment: in our application, we will align the GRIN lens with the irradiated microoptics by placing it in a groove in the milled base plate, which will also support the irradiated optical system, as explained in the introduction.

In Fig. 6, we show the dimensions of the simulated system. The MMF detector is positioned at the focus in the *yz*-plane of the GRIN lens (SELFOC SLW2.0, with a pitch of 0.28 at 409 nm). In the *xz*-plane, we can optimize the radius of curvature of the cylindrical microlens between the capillary and the GRIN lens, to focus the light also in this plane at the same position. Simulations show that for a focal length of 1000 μm,

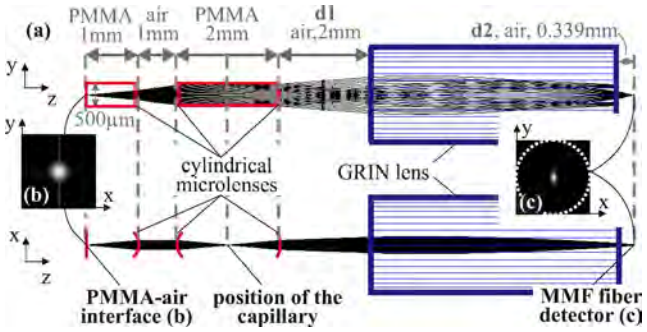

Fig. 6. (a) Schematic representation of the simulated setup and the obtained energy distribution of (b) the source (measurement area of 25 μm $\times$ 25 μm) and (c) on the MMF fiber tip (measurement area of 50 μm $\times$ 50 μm) (white = highest energy and black = lowest energy values).

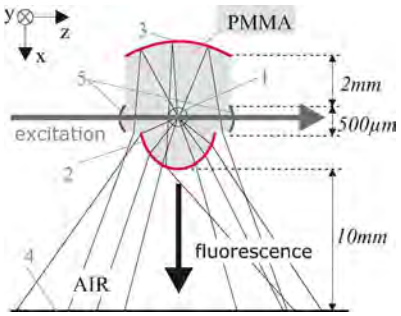

Fig. 7. (a) Schematic representation with ray tracing of the simulated setup for fluorescence detection (not on scale) (1 = capillary with fluorescent molecules, 2 = cylindrical microlens for fluorescence collection, 3 = extra-bended surface, 4 = detector, 5 = cylindrical microlenses for excitation and absorption measurement).

the best focus onto the MMF is achieved and so the integrated energy distribution on the detector [Fig. 6(c)] divided by the integrated energy distribution of the source [Fig. 6b] is maximal: 99.7% for ideal transmitting lens surfaces and 75% when Fresnel reflections are taken into account.

C. Fluorescence

We implement an orthogonal setup for the fluorescence detection, meaning that the direction in which fluorescence is collected and the direction of the light path of the excitation light are perpendicular to each other. This is also illustrated in Fig. 7, where the components for fluorescence collection (surfaces 2 and 3, and detector 4) are positioned along the direction perpendicular to the microlenses for excitation and absorption measurement (5) and to the capillary (1).

In the center of the capillary, we put the source: an emitting elongated spheroid with a length of 100 μm, filling the complete inner diameter of the capillary and representing a small fluorescent plug of molecules propagating in the capillary. The 100 μm value was chosen because this is the length of the smallest plugs we want to be able to detect. The wavelength of the source was set to 480 nm, the emission peak of coumarin 480—the fluorescent dye we will use in the experiments—when excited at 409 nm. Without any collimating optics, the efficiency, defined as the

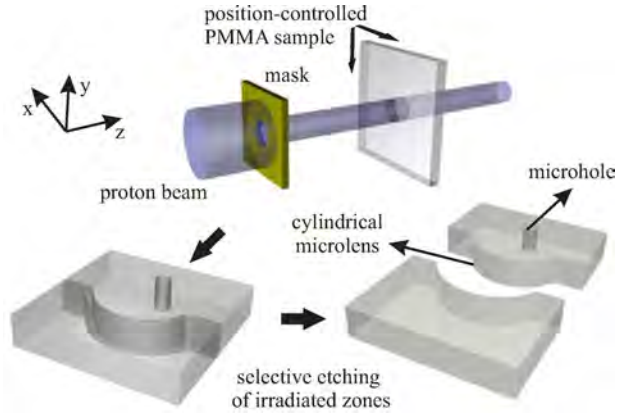

Fig. 8. Basic processing steps of DPW: Patterning of a polymer photoresist through proton irradiation, followed by chemical etching of the irradiated zones using a specific developer.

amount of power measured by the detector divided by the amount of power emitted by the source representing the fluorescent plug, is only 6.7%, taking into account Fresnel reflections in the system. Therefore, we introduce a cylindrical microlens and an extra-bended surface at the opposite side of the capillary, to collect more fluorescent light. At the latter surface, light rays will be reflected by means of total internal reflection and they will propagate back through the capillary and the fluorescence collection microlens toward the detector. The distance between the detector and the microlens is 1 cm to account for the housing of the detector around the sensor. The radius of curvature of the microlens and the bended surface and the distance between these curvatures and the center of the capillary are the variables in the system that should be optimized. Simulations show that an efficiency of 13.7% is achieved by means of a microlens with a radius of curvature of 701 μm, which is positioned on a distance of 320 μm away from the center of the capillary, and a bended surface with a radius of curvature of 1885 μm positioned at a distance of 1220 μm away from the center of the capillary. The latter distance is larger to provide mechanical stability to the component. If we place a flat external mirror 1 mm behind the extra-bended surface to reflect more light, the efficiency increases to 20.1%.

III. Fabrication of the Microoptical Component

For the fabrication of the microoptical component, we use DPW, a technology to rapidly prototype microoptical systems that can combine micromechanical positioning structures and refractive microoptical components such as microholes, microlenses, microprisms, and cylindrical microlenses [24], [25].

The DPW process consists of the following basic procedures, as illustrated in Fig. 8. First, a collimated 8.3 MeV proton beam is used to irradiate an optical-grade PMMA sample according to a predefined pattern by translating the PMMA sample perpendicularly to the proton beam. We use PMMA samples with a thickness of 500 μm, which allows the 8.3 MeV protons to completely traverse the sample. This irradiation step causes scissions in the long, high molecular weight polymer chains, and as a consequence, the molecular weight of the material located

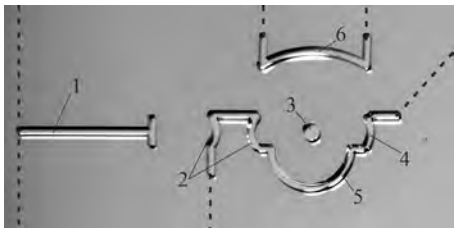

Fig. 9. Irradiated and etched component (1 = fiber groove, 2 = microlenses to focus the excitation light, 3 = hole to insert the capillary, 4 = microlens to capture nonabsorbed excitation light, 5 = microlens to collect fluorescence and 6 = extra bended surface, dotted lines will be milled).

in the irradiated zones will be reduced and free radicals will be created, resulting in material properties that are different from those of the bulk. These changes can be exploited in the next process step, in which a selective etching solvent is applied for the development of the irradiated zones. This allows for the fabrication of (2-D arrays of) microholes, cylindrical microlenses, and optically flat micromirrors (with a typical rms surface roughness below 30 nm over an area of 48 μm $\times$ 60 μm), as well as alignment features and mechanical support structures. For the microfabricated part in our detection setup, we irradiate the contours of the design and then etch the sample. However, to limit the total irradiation time, we only pattern and etch the contours of the microlenses, the fiber groove, and the hole for the capillary (Fig. 9). The other surfaces do not need optical quality and are milled after the etching step to release the detection component (dotted lines in Fig. 9). The final component is as shown earlier in Fig. 2. Although DPW is not a mass fabrication technique as such, one of its assets is that once the master component has been prototyped, a metal mould can be generated from the DPW master by applying electroplating. After removal of the plastic master, this metal mould can be used as a shim in a final microinjection moulding or hot embossing step [26]. This way, the master component can be mass produced at a low cost in a variety of high-tech plastics.

IV. Proof-of-Concept Demonstration

Finally, the fabricated component is used and its performance is characterized in a proof-of-concept demonstration setup. The complete setup (Fig. 10) consists of the following main parts: the source and the coupling of the excitation light in a single-mode optical fiber, the valve and fused silica capillary tubing to bring the sample to the detection unit, the microoptical component (Fig. 11), the absorbance detection part and the fluorescence detection part.

A. Description of the Experimental Setup

1) Excitation Light Source: To excite the molecules in the fluidic channel we use an InGaAsP semiconductor laser, emitting 14.3 mW at a wavelength of 409 nm. The light is coupled into a single-mode optical fiber (Corning SMF-28 optical fiber). Five milliwatts or 35% of the light emitted by the laser is available at the end of the optical fiber. Losses are due to manual fiber coupling and the absorption of the blue light in the optical fiber,

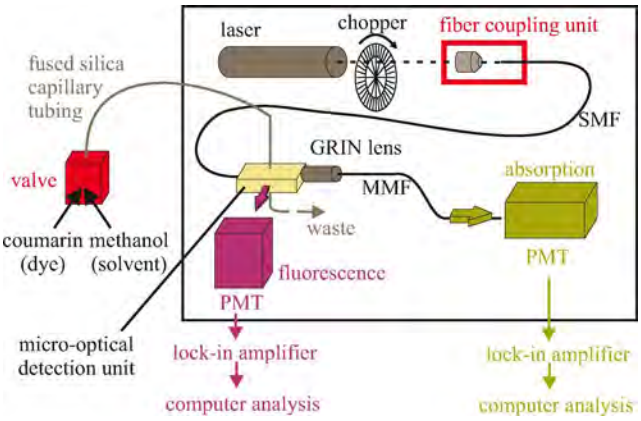

Fig. 10. Schematic overview of the proof-of-concept demonstration setup.

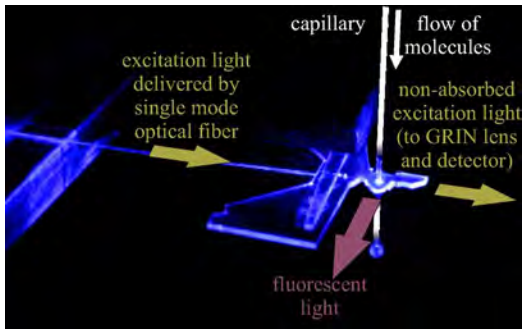

Fig. 11. Picture of the microoptical component with the optical fiber that delivers the excitation light and the fused silica capillary to deliver the sample to the detection unit.

which is optimized for use at near-IR telecom wavelengths. Nevertheless, 5 mW will be sufficient to excite the molecules in the capillary—larger intensities could cause photobleaching of the fluorescent molecules. The free end of the optical fiber is fixed on an *xyz*-translation stage and is inserted in the fiber groove in the microoptical detection unit. As such, it is automatically aligned with the rest of the microoptical system. Before insertion, a drop of index matching gel was applied on the fiber tip. Consequently, a gel layer is constituted after completion of the insertion between the fiber tip and the groove end facet, which avoids scattering at this interface.

2) Chemical Sample: For the characterization of the system, we use a fluorescent dye, coumarin 480, that absorbs the 409 nm excitation light and that has a good quantum efficiency, and as such, a high fluorescence yield. All the samples used for fluorescence and absorbance measurements are prepared from stock solution consisting of 60 mM coumarin dye dissolved in methanol. Samples at lower concentrations are prepared by dilution of the stock solution with methanol.

A fused silica capillary is inserted in the hole in the microoptical component. Index matching gel is applied to avoid scattering at air gaps between the outer side of the capillary and the inside of the hole. The capillary is connected to a switching valve. Two syringes are connected to the valve, one containing methanol and the other one containing the dye solution. By switching the valve, methanol and the solution can be injected

repeatedly with a minimal dead volume between consecutive injections. Injection was performed manually by means of the syringes.

First, we will study the response of the detection system on a step from methanol to dye solution and back (e.g., inject 100 μL of methanol, switch and inject 100 μL of dye solution, switch back and inject again 100 μL of methanol). Before a series of measurements with a certain concentration is started, the capillary and the valve are rinsed thoroughly with at least 2 mL pure methanol. In the first stage, a capillary with an inner diameter of 150 μm is used.

3) Absorbance Detection System: A SELFOC SLW2.0 GRIN lens is positioned behind the microoptical component to collect the nonabsorbed excitation light at 409 nm. The collected light is then focused into an MMF (0.48-NA hard polymer clad multimode fiber), which is fixed on an *xyz*-translation stage. When the capillary is filled with methanol, which is not absorbing light at 409 nm, 0.8 mW is available at the output of the MMF. This means that only 16% of the excitation light emitted by the SMF (5 mW) used for excitation of the molecules in the capillary, is available at the output of the MMF. Losses are due to manual fiber coupling, to the absorption of the blue light in the optical fiber, which is optimized for use at near-IR telecom wavelengths, and to scattering of the excitation light in the microoptical component at interfaces between PMMA and air and at the interface with the capillary. A photomultiplier tube (PMT) is used for the quantitative detection of the light at the output of the MMF. To avoid saturation or even damage of the PMT due to this intense laser light, a neutral density filter with an optical density (OD) of 0.3 (50% transmission) is placed in front of the PMT. In addition, a D405/10 exciter filter is used to select only the excitation light and to block fluorescent light at higher wavelengths. Both filters are placed as close as possible to the PMT to prevent the pick-up of noise from scattered light in the system.

4) Fluorescence Collection System: The fluorescence light is transferred consecutively through the fluorescence collecting microlens in the microoptical detection unit, a diaphragm and a filter, toward the PMT. To increase the efficiency, an external mirror is placed behind the capillary to reflect part of the light that would otherwise leave the setup in that direction. This light will propagate back through the capillary and will also be collected by the microlens. The orthogonal fluorescence detection setup provides a geometrical separation of excitation light and fluorescence emission. In theory a filter is not necessary, yet, in practice, scattering of the excitation light will occur and additional spectral filtering of the fluorescence emission is needed. We use a coumarin D460/50 emitter filter. The filter is placed as close as possible to the detection area of the PMT to avoid the detection of scattered excitation light.

5) Data Analysis: An optical chopper was placed at the output of the laser to modulate the excitation light and the PMTs used for both absorbance and fluorescence detection were coupled to a lock-in amplifier. By this, the detection of noise signals in the system and its surroundings, is minimized. The resulting data of the lock-in amplifier were acquired by means of LabVIEW software, at a sample of rate 10 Hz (10 samples/s). Afterward, the data was further processed by means of Matlab software.

B. Results and Discussion

The performance of a detection system is defined by means of the limit of detection (LOD), i.e., the smallest concentration of an analyte for which we can decide whether that analyte is present or not in the sample under test. So, although the detection system will sometimes detect smaller concentrations of that analyte than the LOD, the LOD represents the smallest concentration that indicates the "true" detection capability of the system. The LOD is mathematically expressed as the concentration C_{LOD} and will be derived from the voltage signal, S_{LOD}, generated by the PMT, which converts optical power into a voltage signal.

The critical level C_C, is the concentration above which the decision "detected" is made. This level corresponds to the minimal significant signal (S_C) that can be distinguished from the noisy background signal. The background is measured by injecting nonfluorescent molecules in the channel (methanol, $C = 0$) and measuring the resulting signals for a sufficiently long period in time (in our experiments at least 300 measurement points). The resulting signals for the background are distributed about the mean value S_B, with a standard deviation σ_B. S_C should be significantly higher than S_B. Statistically, we can state that the probability for a false positive (α, type 1 error) at the critical level should be low. A value of 0.05 for α is recommended by the International Union of Pure and Applied Chemistry (IUPAC) [27]. To indicate the inherent "true" detection capability of the detection system, we should also take into account the distribution of the measurements of the signal level corresponding to the detection limit concentration (mean value S_{LOD} and standard deviation σ_{LOD}). S_{LOD} should be sufficiently larger than S_C to have a significant certainty that concentration C_{LOD} will be detected, and therefore, to define it as the detection limit. Statistically, we can state that the probability of a false negative (β, type 2 error) should be low and again a value of 0.05, for β is recommended by the IUPAC [27]. If S_{LOD} and S_B are normally distributed and if the variance is constant between $C = 0$ and $C = C_{\mathrm{LOD}}$, the signal corresponding to the limit of detection can be obtained as [28]

$$S_{\mathrm{LOD}} = 3.3 \times \sigma_B + S_B \tag{1}$$

The correlation between concentrations C and the corresponding voltage signal levels S can be found experimentally by injecting samples with different concentrations of that molecule dissolved in methanol in the fused silica capillary and by fitting these results to obtain a calibration curve. To find the limit of detection in concentration units, the calibration curve can be used to convert S_{LOD} to the corresponding concentration C_{LOD}.

In the following paragraphs, we investigate the detection limit for both the fluorescence and the absorbance detection system. We will inject samples with different concentrations of coumarin dissolved in methanol, in the fused silica capillary with an inner diameter of 150 μm. Large sample plugs are injected for these sensitivity measurements, so that the dispersion effects do not

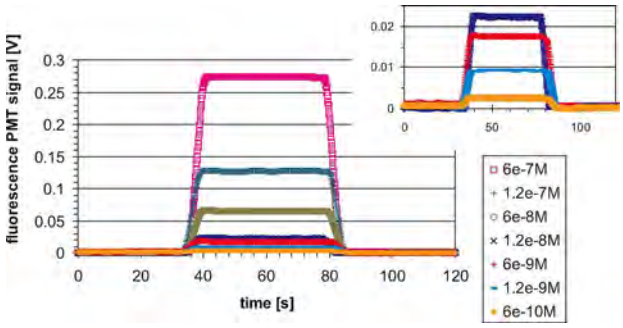

Fig. 12. Experimental data obtained for plugs with different molar concentrations. For every concentration, one measurement is shown (no averaging of different samples). The raw data were filtered by means of a 20-point low-pass boxcar filter.

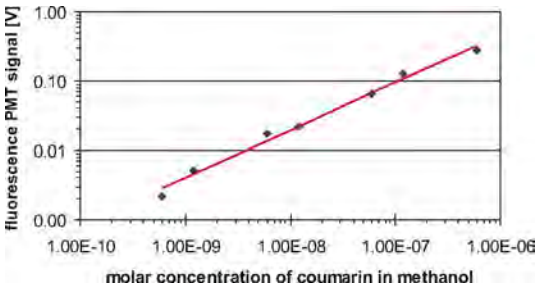

Fig. 13. Mean value of the background-corrected signal as a function of the molar concentration of the injected sample (every time ten measurements).

cause dilution of the maximum achievable sample absorbance and fluorescence. A calibration curve will be constructed and by analyzing the background noise distribution obtained for methanol without coumarin in the capillary, we will be able to estimate the detection limit by means of (1). However, the detection limit can also be obtained experimentally. Therefore, we will inject gradually lower concentrations of the coumarin in the microchannel, and for every concentration, we will calculate the SNR of the resulting voltage signal. The SNR is defined as

$$\text{SNR} = \frac{S - S_B}{\sigma_B} \tag{2}$$

where S is the mean value obtained for the concentration under test. The concentration for which the SNR equals 3.3 can be defined as the experimentally obtained LOD, and we will compare the latter with the theoretically obtained LOD.

1) Fluorescence Analysis: In Fig. 12, we show examples of results obtained for fluorescence measurements on samples with different molar concentrations. For every concentration prepared, ten consecutive injections were performed. In Fig. 13, the mean value of the background-corrected signal ($=S - S_B$) as a function of the concentration is shown graphically. In Table I, we calculate the average values resulting from every set of ten injections, and we summarize the SNR and the background-corrected signal $S - S_B$. The average background signal S_B represents the systematic errors in our fluorescence measurement setup. Ideally, S_B would be zero, but, in practice, a small amount of excitation light at 409 nm will also be detected as the filter

TABLE I
SNR AND AVERAGE BACKGROUND-CORRECTED SIGNAL FOR DIFFERENT MOLAR CONCENTRATIONS

Molar Concentration	SNR	S-S_B [V]
6e-7M	1075	0.27764
1.2e-7M	663	0.12628
6e-8M	296	0.06544
1.2e-8M	108	0.02148
6e-9M	93	0.01704
1.2e-9M	37	0.00523
6e-10M	18	0.00215

TABLE II
SNR AND AVERAGE BACKGROUND-CORRECTED SIGNAL FOR DIFFERENT MOLAR CONCENTRATIONS (FILTERED DATA)

Molar Concentration	SNR	S-S_B [V]
6e-7M	1266	0.27764
1.2e-7M	1127	0.12629
6e-8M	470	0.06544
1.2e-8M	168	0.02146
6e-9M	161	0.01704
1.2e-9M	50	0.00524
6e-10M	29	0.00214

we use to select wavelengths higher than 409 nm is not perfect. The average background noise σ_B for the measurements is 220 μV. This noise is representing stochastic variations, e.g., due to instability of the excitation source, shot noise, and Johnson noise in the electronic circuity.

We applied a 20-point low-pass boxcar filter on all acquired data to reduce the noise. The results of the analysis of these filtered data are summarized in Table II (average values resulting from every set of ten injections). By means of the filtering, we are able to decrease the average background noise σ_B to 150 μV and to increase the SNR, on average, with a factor of 1.5. We remark that the length of the boxcar filter should be chosen carefully when small sample plugs are characterized by the system, as the filter could cause smoothing of the small intensity peaks resulting in incorrect intensity measurements. Therefore, when the system will be used to detect small samples at high flow rates, we will search for a tradeoff between noise filtering and the smallest sample plug that can be characterized by the system.

As the measured signals were normally distributed around their mean values, we can estimate the detection limit by means of (1) and the obtained values for the background noise σ_B, and the obtained calibration curve. This theoretically obtained LOD equals 80 pM and 60 pM for the raw data and the filtered data, respectively. However, the smallest concentration we were able to detect experimentally equals 600 pM, one order of magnitude higher than the theoretically obtained LOD. For small concentrations, it is more difficult to assure that the concentration of the sample flowing in the microchannel is equal to the concentration intended to measure. Indeed, with every dilution step, a small error is introduced due to the preparation of the sample and the prepared concentration will deviate slightly from the one that was intended to prepare. For the smallest concentrations,

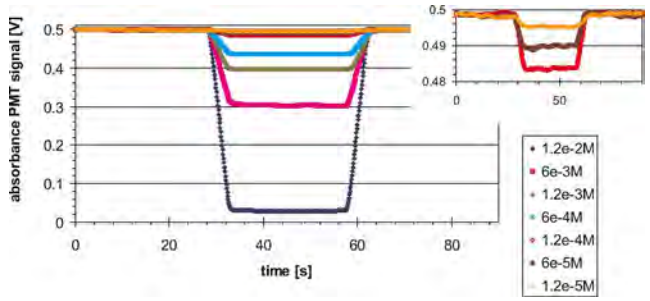

Fig. 14. Experimental data obtained for plugs with different molar concentrations. For every concentration, one measurement is shown (no averaging of different samples). The raw data were filtered by means of a 20-point low-pass boxcar filter.

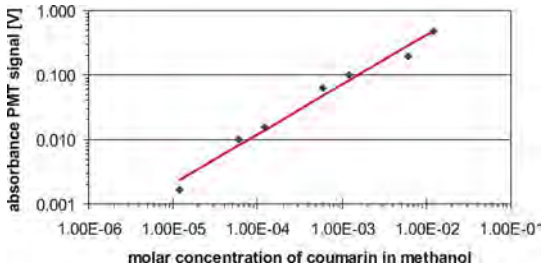

Fig. 15. Mean value of the decrease of the voltage signal as a function of the molar concentration of the injected sample (every time ten measurements).

several dilution steps are needed, and so, the resulting error will be larger than for higher concentrations. In addition, coumarin tends to crystallize in the valve or in the microchannel when no liquid is flowing in the setup. Although the valve and the channel were always rinsed thoroughly with pure methanol before every measurement session, a small amount of this crystallized material could remain in the valve or channel. When it dissolves during a measurement, the concentration of the sample under test will slightly increase. For samples with high concentrations, this will not be visible in our results, but for the smallest concentrations, this could affect the measurement. For samples with concentrations below 600 pM, the fluorescence measurements were not repeatable anymore due to the errors described earlier. Therefore, the experimental LOD is set to 600 pM.

For concentrations above 0.6 μM, the measured signals do not follow the linear calibration curve anymore and saturation of the PMT voltage level takes place.

2) Absorbance Analysis: In the absorbance detection part, we measure the amount of nonabsorbed excitation light that is passed through the system, and hence, we can calculate the absorption of the sample. To investigate the LOD of the absorbance detection system, we inject samples with different concentrations of the coumarin dye dissolved in methanol in the fused silica capillary and then measure the corresponding decrease in the PMT voltage with respect to the signal obtained for pure methanol. We will still call this signal S_B to stay consistent with the terminology and formulas described earlier, but we keep in mind that S_B will be higher than the signals obtained for coumarin samples, as it represents the amount of excitation light that is passed through the system when no absorption takes place. In Fig. 14, we show examples of results obtained for samples with different molar concentrations.

For every concentration prepared, ten consecutive injections were performed. In Fig. 15, the mean value of the decrease of the voltage signal $S_B - S$ as a function of the concentration is shown graphically. In Table III, we calculate the average values resulting from every set of ten injections, and we summarize the SNR and the decrease of the voltage signal $S_B - S$. The average background noise σ_B for these measurements is 1860 μV. We applied a 20-point low-pass boxcar filter on all acquired data to reduce the noise. The results of the analysis of these filtered

TABLE III
SNR AND DECREASE OF THE VOLTAGE SIGNAL FOR DIFFERENT MOLAR CONCENTRATIONS

Molar Concentration	SNR	$S_B - S$ [V]
1.2e-2M	801	0.46809
6e-3M	379	0.19462
1.2e-3M	157	0.09946
6e-4M	108	0.06328
1.2e-4M	33	0.01534
6e-5M	14	0.00989
1.2e-5M	3	0.00165

TABLE IV
SNR AND DECREASE OF THE VOLTAGE SIGNAL FOR DIFFERENT MOLAR CONCENTRATIONS (FILTERED DATA)

Molar Concentration	SNR	$S_B - S$ [V]
1.2e-2M	1001	0.46804
6e-3M	560	0.19461
1.2e-3M	224	0.09946
6e-4M	172	0.06328
1.2e-4M	58	0.01535
6e-5M	21	0.00992
1.2e-5M	5	0.00165

data are summarized in Table IV (average values resulting from every set of ten injections). By means of the filtering we are able to decrease the average background noise σ_B to 1390 μV and to increase the SNR on average with a factor of 1.5. Again, the length of the filter should be optimized when the system is used to detect small samples at high flow rates.

The resulting theoretically obtained LOD equals 9 μM and 6 μM for the raw data and the filtered data, respectively. The smallest concentration we were able to detect experimentally equals 12 μM, which is very close to the theoretically predicted values. The concentrations studied in these absorption measurements (12 μM–12 mM) are larger then those investigated in the fluorescence detection experiments (600 pM–0.6 μM). For these large concentrations, we do not have the problems with errors caused by repeated dilution or uptake of crystallized coumarin in the system, and therefore, it is easier to reach the theoretically calculated LOD by means of experiments.

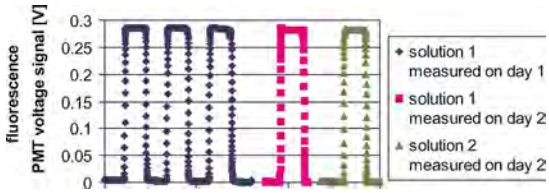

Fig. 16. Repeatability of fluorescence detection measurements: comparison of the results of 3 consecutive sample injections of a 6e-7M solution diluted from a stock solution prepared by operator 1 (solution 1 on day 1), a measurement result obtained on a different day from a sample taken from the same solution (solution 1 on day 2) and a measurement obtained from a sample from another 6e-7M solution, diluted from a stock solution prepared by operator 2 (solution 2 on day 2).

As the measurement of absorbance implies the measurement of small-signal dips in a high signal level, the LOD for absorbance will always be higher than the one for fluorescence as the SNR for absorbance is inherently larger due to the higher shot noise corresponding to the high signal level. Therefore, we should not put large efforts to lower the absorbance LOD to the lowest value possible, but instead, it makes more sense to use for different concentrations, the most efficient measurement approach, and to make the absorbance and fluorescence parts complementary to be able to measure a concentration range as large as possible with the complete detection unit. In our system, we should try to lower the LOD for absorbance to 0.6 μM, so that it fits to the concentration range covered by fluorescence detection.

For concentrations above 12 mM, the measured signal does not follow the linear calibration curve anymore due to quenching effects.

3) Repeatability: Finally, we will discuss briefly the repeatability of our system. In Fig. 16, we show the fluorescence detection results of three consecutive injections of a 6e-7M solution. This 6e-7M solution was obtained by diluting a 60 mM stock solution, which was prepared by operator 1. After every fluorescence peak, the signal decreases again to the background level, and for every fluorescence peak the signal level is comparable.

On the next day, a sample was taken from the same solution and the resulting fluorescence was investigated. On the same day, a sample of another 6e-7M solution was analyzed by means of the system. This second 6e-7M solution was obtained by diluting a 60 mM stock solution, which was prepared by operator 2. The boxcar filtered measurement signals are summarized in Fig. 16 and the calculated results in Table V. In all measurements, a 6e-7M solution was injected into the channel and a sample with that concentration should always result in a comparable change of the voltage signal. Therefore, we compare in Table V, the resulting background-corrected signals $S_B - S$: in the 2nd column, we give the absolute values, and in the 3th column, we calculate the difference with respect to the value obtained for solution 1 measured on day 2. Only small differences in the 4th significant digit can be observed. In addition, the background noise σ_B in all measurements should be comparable, as this value determines the LOD and the performance of the system. In Table V, we summarize the values of σ_B and the LODs obtained from the filtered measurement signals, and in the last column, we calculate the difference with respect to the LOD obtained for solution 1 measured on day 2. The difference between the measurements of the same solution on different days is only 3.9 pM (7% of the earlier calculated LOD of the system for filtered signals (60 pM)), and therefore, acceptable. The difference between the measurements of samples taken from different solutions on the same day is larger and equals 14% of the calculated LOD of the system (60 pM). However, these are preliminary results for a very limited set of measurements, and in the future, a more extensive repeatability study will be performed to decide with more confidence if for a larger set of different solutions the difference between measurements is acceptable.

TABLE V
REPEATABILITY OF FLUORESCENCE DETECTION MEASUREMENTS

Solution	S_B-S [V]	Δ [V]	σ_B [V]	LOD [pM]	Δ [pM]
#1, day 1	0.2813	*0.0002*	0.000190	67.2	*3.9*
#1, day 2	0.2811	*0*	0.000182	63.3	*0*
#2, day 2	0.2808	*0.0003*	0.000198	71.4	*8.1*

V. CONCLUSION AND FUTURE PERSPECTIVES

Miniaturized and integrated on-chip plastic detection units are needed for the development of portable, robust, and ultimately disposable lab-on-a-chip devices. We have developed a detection system combining both laser-induced fluorescence and absorbance analysis, which can be used for chromatographic applications in fused silica capillaries. The detection system contains a plastic microfabricated part with integrated optics, which are directly aligned onto the microfluidic channel. An additional GRIN lens, filters, an excitation source, and two PMT detectors complete the detection unit.

We designed the detection system by means of nonsequential ray tracing simulations and the microfabricated part was prototyped by means of DPW. This technology is compatible with standard replication techniques such as injection molding and hot embossing, which makes our prototypes suitable for low-cost mass production.

The microfabricated detection part was used in a proof-of-concept demonstration setup, where we investigated the detection limit LOD for both the absorbance and fluorescence detection part. Samples with various concentrations of coumarin dyes were injected in a capillary with an inner diameter of 150 μm and a calibration curve was constructed giving the correlation between the concentration of the sample and the resulting PMT voltage signal. The detection limit was estimated both theoretically by means of the background noise and experimentally (SNR $=$ 3.3). For the absorbance detection, the average background noise σ_B measured 1390 μV with a resulting LOD of 6 μM. The smallest concentration we were able to detect experimentally equals 12 μM, which is very close to the theoretically obtained value. For the fluorescence detection, the average background noise σ_B in the measurements was 150 μV and the resulting theoretically obtained LOD equaled 60 pM. However, the smallest concentration we were able to detect experimentally equals 600 pM, one

order of magnitude higher than the theoretically obtained LOD. We detected concentrations ranging from 600 pM to 0.6 μM by means of fluorescence detection and concentrations ranging from 12 μM to 12 mM by means of absorbance measurements.

In the future, we will try to lower the background noise to increase the performance of the system and to reach lower LODs, by using detectors and an excitation source with the optimal properties for our application and by improving the collection of the light in the microfabricated system. In addition, we will investigate the repeatability of our system in more detail, then we will optimize our system for the detection of smaller plugs flowing at higher rates in the microchannel, and finally, we will couple the detection setup to a chromatographic column to investigate the analysis of real chromatographic separations.

In this paper, we presented the proof-of-concept of the proposed detection configuration by using capillaries that can be easily replaced, but ultimately, the goal will be to adapt this detection approach for the detection of fluorescence and/or absorption in on-chip microchannels with inner diameters ranging from a few micrometers up to 100 μm and special geometries like *Z*-cells to increase the optical path length at the detection point. In addition, we will try to adapt the design to enable high-throughput parallel detection by means of different detection units on one chip. Chromatographic separations will then be carried out on the same microfluidic chip, by which a true μTAS system can be created.

VI. Acknowledgment

The authors would like to thank P. Vynck, Y. Meuret, and the members of the DPW team and the Department of Chemical Engineering of the Vrije Universiteit Brussel.

References

[1] A. Manz, N. Graber, and H. M. Widmer, "Miniaturized total chemical analysis systems: A novel concept for chemical sensing," *Sens. Actuators, B, Chem.*, vol. 1, pp. 244–248, 1990.

[2] P. S. Dittrich, K. Tachikawa, and A. Manz, "Micro total analysis systems. Latest advancements and trends," *Anal. Chem.*, vol. 78, pp. 3887–3907, 2006.

[3] J. C. Fister, S. C. Jacobson, L. M. Davis, and J. M. Ramsey, "Counting single chromophore molecules for ultrasensitive analysis and separations on microchip devices," *Anal. Chem.*, vol. 70, pp. 431–437, 1998.

[4] G. Jiang, S Attiya, G. Ocvirk, W. E. Lee, and D. J. Harrison, "Red diode laser induced fluorescence detection with a confocal microscope on a microchip for capillary electrophoresis," *Biosens. Bioelectron.*, vol. 14, pp. 861–869, 2000.

[5] J. Fu, Q. Fang, T. Zhang, X. Jin, and Z. Fang, "Laser-induced fluorescence detection system for microfluidic chips based on an orthogonal optical arrangement," *Anal. Chem.*, vol. 78, pp. 3827–3834, 2006.

[6] E. Thrush, O. Levi, W. Ha, G. Carey, L. J. Cook, J. Deich, S. J. Smith, W. E. Moerner, and J. S. Harris, "Integrated semiconductor vertical-cavity surface-emitting lasers and PIN photodetectors for biomedical fluorescence sensing," *J. Quantum Electron.*, vol. 40, no. 5, pp. 491–498, 2004.

[7] V. Namasivayam, R. Lin, B. Johnson, S. Brahmasandra, Z. Razzacki, D.T Burke, and M. A Burns, "Advances in on-chip photodetection for applications in miniaturized genetic analysis systems," *J. Micromech. Microeng.*, vol. 14, pp. 81–90, 2004.

[8] S. Qi, X. Liu, S. Ford, J. Barrows, G. Thomas, K. Kelly, A. McCandless, K. Lian, J. Goettertc, and S. A. Soper, "Microfluidic devices fabricated in poly(methyl methacrylate) using hot-embossing with integrated sampling capillary and fiber optics for fluorescence detection," *Lab. Chip*, vol. 2, pp. 88–95, 2002.

[9] J. C. Roulet, R. Volkel, H. P. Herzig, E. Verpoorte, N. F. de Rooij, and R. Dandliker, "Performance of an integrated microoptical system for fluorescence detection in microfluidic systems," *Anal. Chem.*, vol. 74, pp. 3400–3407, 2002.

[10] P. Norlin, O. Öhman, B. Ekström, and L. Forssén, "A chemical micro analysis system for the measurement of pressure, flow rate, temperature, conductivity, UV-absorption and fluorescence," *Sens. Actuators, B, Chem.*, vol. 49, pp. 34–39, 1998.

[11] H. Li, J. Lin, R. Su, K. Uchiyama, and T. Hobo, "A compactly integrated laser-induced fluorescence detector for microchip electrophoresis," *Electrophoresis*, vol. 25, pp. 1907–1915, 2004.

[12] K. Uchiyama, W. Xu, J. Qiu, and T. Hobo, "Polyester microchannel chip for electrophoresis—incorporation of a blue LED as light source," *Fresnius J. Anal. Chem.*, vol. 371, pp. 209–211, 2001.

[13] J. Johansson, T. Johansson, and S. Nilsson, "Fluorescence imaging of light absorption for axial-beam geometry in capillary electrophoresis," *Electrophoresis*, vol. 19, no. 12, pp. 2233–2238, 1998.

[14] P. Lindberg, A. Hanning, T. Lindberg, and J. Roeraade, "Fiber-optic-based UVvisible absorbance detector for capillary electrophoresis, utilizing focusing optical elements," *J. Chromatogr. A*, vol. 809, pp. 181–189, 1998.

[15] H. Wang, E. C. Yi, C. A. Ibarra, and M. Hackett, "A remote flow cell for UV absorbance detection with capillary HPLC based on a single strand fiber optic," *Analyst*, vol. 125, pp. 1061–1064, 2000.

[16] G. E. Collins and Q. Lu Lu, "Radionuclide and metal ion detection on a capillary electrophoresis microchip using LED absorbance detection," *Sens. Actuators, B, Chem.*, vol. 76, pp. 244–249, 2001.

[17] T. Tsuda, J. V. Sweedler, and R. N. Zare, "Rectangular capillaries for capillary zone electrophoresis," *Anal. Chem.*, vol. 62, pp. 2149–2152, 1990.

[18] Y. Xue and E. S. Yeung, "Characterization of band broadening in capillary electrophoresis due to nonuniform capillary geometries," *Anal. Chem.*, vol. 66, pp. 3575–3580, 1994.

[19] E. Verpoorte, A. Manz, H. Ldi, A. E. Bruno, F. Maystre, B. Krattiger, H. M. Widmer, B. H. van der Schoot, and N. F. de Rooij, "A silicon flow cell for optical detection in miniaturized total chemical analysis systems," *Sens. Actuators B, Chem.*, vol. 6, pp. 66–70, 1992.

[20] Z. Liang, N. Chiem, G. Ocvirk, T. Tang, K. Fluri, and D. J. Harrison, "Microfabrication of a planar absorbance and fluorescence cell for integrated capillary electrophoresis devices," *Anal. Chem.*, vol. 68, pp. 1040–1046, 1996.

[21] H. Salimi-Moosavi, Y. Jiang, L. Lester, G. McKinnon, and D. J. Harrison, "A multireflection cell for enhanced absorbance detection in microchip-based capillary electrophoresis devices," *Electrophoresis*, vol. 21, pp. 1291–1299, 2000.

[22] K. W. Ro, K. Lim, B. C. Shim, and J. H. Hahn, "Integrated light collimating system for extended optical-path-length absorbance detection in microchip-based capillary electrophoresis," *Anal. Chem.*, vol. 77, pp. 5160–5166, 2005.

[23] Breault Research Organization, Inc. [Online]. Available: www.breault.com (accessed on Jul. 27, 2007).

[24] C. Debaes, J. Van Erps, M. Vervaeke, B. Volckaerts, H. Ottevaere, V. Gomez, P. Vynck, L. Desmet, R. Krajewski, Y. Ishii, A. Hermanne, and H. Thienpont, "Deep proton writing: A rapid protoyping polymer microfabrication tool for micro-optical modules," *New J. Phys.*, vol. 8, pp. 270–288, 2006.

[25] H. Ottevaere, B. Volckaerts, M. Vervaeke, P. Vynck, A. Hermanne, and H. Thienpont, "Plastic microlens arrays by deep lithography with protons: Fabrication and characterization," *Jpn. J. Appl. Phys.*, vol. 43, no. 8B, pp. 5832–5839, 2004.

[26] M. Heckele and W. K. Schomburg, "Review on micro molding of thermoplastic polymers," *J. Micromech. Microeng.*, vol. 14, pp. R1–R14, 2004.

[27] IUPAC, in *Compendium of Analytical Nomenclature*, J. Inczedy, T. Lengyel, A. M. Ure, A. Gelencser, and A. Hulanicki, Eds., 3rd ed. Oxford, U.K.: Blackwell, 1998.

[28] L. A. Currie, "Detection and quantification limits: Origins and historical overview," *Anal. Chim. Acta*, vol. 391, pp. 127–134, 1999.

Sara Van Overmeire was born in Halle, Belgium, in 1982. She received the Master degree in electrotechnical engineering with majors in photonics from the Vrije Universiteit Brussel (VUB), Brussels, Belgium, in 2005, where she was engaged in research on the detection of fluorescence in DNA microarrays. Since October 2005, she is working toward the Ph.D. degree at the Department of Applied Physics and Photonics (FirW-TONA), VUB, with a fellowship from the Flemish Fund for Scientific Research.

Her current research interests include biophotonics, with an emphasis on the integration of small fluorescence detection modules on microchannels and DNA microarrays.

Heidi Ottevaere was born in Halle, Belgium, on January 21, 1974. She received the Master degree in electrotechnical engineering with majors in photonics and the Ph.D. degree in applied sciences from the Vrije Universiteit Brussel (VUB), Brussels, Belgium, in 1997 and 2003, respectively.

In 1997, she joined the Department of Applied Physics and Photonics (FirW-TONA), VUB, as a Teaching Assistant, where she is currently engaged in research on optical fiber sensing, where she demonstrated a novel method to characterize dental resin cements. She was an invited speaker at the SPIE "Photonics Europe" Conference in Strasbourg, France, in 2004. She is currently supervising several microoptical industry-oriented research projects. Recently, she also initiated together with her colleagues a research group on biophotonics with assistance from different European top-research groups. She is also a promoter or copromoter of some basic research projects, which are financially supported by regional and national bodies such as the Fund for Scientific Research Vlaanderen (FWO) and the Belgian Federal Science Policy Office. She is also a Deputy Workpackage Leader of the "Centre for Measurement and Instrumentation" of the European 6th FP Network of Excellence on Micro-optics "NEMO." She is the author or coauthor of more than 50 papers in international conference proceedings and is the author of two book chapters. She is the holder of one patent. Her current research interests include the optical characterization of microlenses, the fabrication of microlenses with deep proton lithography, in particular, and microoptical instrumentation.

Gert Desmet was born in 1967. He received the Ph.D. degree in chemical engineering from the Vrije Universiteit Brussel, Brussels, Belgium, where he is currently the Professor and Head of the Department of Chemical Engineering (FirW-CHIS).

He is currently leading a research group working on the practical demonstration of the separation speed of shear-driven and pressure-driven flow devices for ultrafast chromatography and for DNA hybridization enhancement. On the theoretical side, his group aims at a better understanding of the relation between the packing structure and the performance of the high-pressure liquid chromatograph. He is currently also leading a 2.6 million Euro initiative of the Flemisch Government on the fabrication of micromachined chromatographic columns. He is the author or coauthor of 70 peer-reviewed papers. He is the holder of five patents. His current research interests include the miniaturization of separation methods and the investigation and the modeling of flow effects in chromatographic systems.

Prof. Desmet is a member of the editorial board of the *Journal of Chromatography A* and a member of the scientific committee of several international conferences. In association with his students, he was the recipient of numerous awards at international conferences for his oral or poster presentations: the Nanotech Montreux in 1999, the Hyphenated Techniques in Chromatography Conference in 2004, the HPLC Conference Series in 2004 and 2006), and the Desty Memorial award in 2006.

Hugo Thienpont (A'97–M'97) was born in Ninove, Belgium, in 1961. He received the Master degree in electrotechnical engineering and the Ph.D. degree in applied sciences from the Vrije Universiteit Brussel (VUB), Brussels, Belgium, in 1984 and 1990, respectively.

In 1994, he was a Professor in the Faculty of Applied Sciences, with teaching responsibilities in photonics. In 2000, he became a Research Director in the Department of Applied Physics and Photonics (FirW-TONA), VUB, and in 2004, he was elected Chair of the Department. Currently, he is coordinating several basic research and networking projects such as the European Network of Excellence on Micro-Optics (NEMO). In addition to academic-oriented research projects, he manages microphotonics-related industrial projects with companies like Barco, Agfa-Gevaert, Tyco, and Umicore. He is the author or coauthor of more than 120 SCI-stated journal papers and more than 400 publications in international conference proceedings. He is the editor of 20 conference proceedings and is the author of five chapters in books. He was an invited speaker at 40 international conferences. He is the holder of ten patents. His current research interests include micro-optics technologies for biophotonic applications, optical interconnects, and photonic sensing.

Prof. Thienpont is a Fellow of the International Society for Optical Engineering (SPIE), and a fellow of the EOS, and a member of the IEEE Laser and Electro-Optics Society (LEOS), and the Optical Society of America (OSA). He served as a Guest Editor of several special issues on Optical Interconnects for the *Applied Optics* and the IEEE JOURNAL OF SELECTED TOPICS ON QUANTUM ELECTRONICS, and is a General Chair of the SPIE Photonics Europe conferences in Strasbourg, France. He was the recipient of the International Commission for Optics Prize ICO'99 and the Ernst Abbe medal from Carl Zeiss, the title of IEEE LEOS Distinguished Lecturer in 2003, the SPIE President's Award for dedicated service to the European Community in 2005, and the MOC Award in 2007.